BMC Medical Imaging

RESEARCH

Open Access

Prediction of acute pancreatitis severity based on early CT radiomics

Mingyao Qi[1], Chao Lu[1], Rao Dai[1], Jiulou Zhang[2], Hui Hu[3*] and Xiuhong Shan[1*]

Abstract

Background This study aims to develop and validate an integrated predictive model combining CT radiomics and clinical parameters for early assessment of acute pancreatitis severity.

Methods A retrospective cohort of 246 patients with acute pancreatitis was analyzed, with a 70%-30% split for training and validation groups. CT image segmentation was performed using ITK-SNAP, followed by the extraction of radiomics features. The stability of the radiomics features was assessed through inter-observer Intraclass Correlation Coefficient analysis. Feature selection was carried out using univariate analysis and least absolute shrinkage and selection operator (LASSO) regression with 10-fold cross-validation. A radiomics model was constructed through logistic regression to compute the radiomics score. Concurrently, univariate and multivariate logistic regression were employed to identify independent clinical risk factors for the clinical model. The radiomics score and clinical variables were integrated into a combined model, which was visualized with a nomogram. Model performance and net clinical benefit were evaluated through the area under the receiver operating characteristic curve (AUC), the DeLong test, and decision curve analysis.

Results A total of 913 radiomics features demonstrated satisfactory consistency. Eight features were selected for the radiomics model. Serum calcium, C-reactive protein, and white blood cell count were identified as independent clinical predictors. The AUC of the radiomics model was 0.871 (95% CI, 0.793–0.949) in the training cohort and 0.859 (95% CI, 0.751–0.967) in the validation cohort. The clinical model achieved AUCs of 0.833 (95% CI, 0.756–0.910) and 0.810 (95% CI, 0.692–0.929) for the training and validation cohorts, respectively. The combined model outperformed both the radiomics and clinical models, with an AUC of 0.905 (95% CI, 0.837–0.973) in the training cohort and 0.908 (95% CI, 0.824–0.992) in the validation cohort. The DeLong test confirmed superior predictive performance of the combined model over both the radiomics and clinical models in the training cohort, and over the clinical model in the validation cohort. Decision curve analysis further demonstrated that the combined model provided greater net clinical benefit than the radiomics or clinical models alone.

Conclusion The clinical-radiomics model offers a novel tool for the early prediction of acute pancreatitis severity, providing valuable support for clinical decision-making.

Keywords Acute pancreatitis, Computed tomography, Radiomics, Nomogram

*Correspondence:
Hui Hu
jshuhui2003@163.com
Xiuhong Shan
13913433095@163.com

[1]Department of Radiology, Affiliated People's Hospital of Jiangsu University, No. 8 Dianli Road, Zhenjiang, Jiangsu, P. R. China
[2]Artificial Intelligence Imaging Laboratory, Nanjing Medical University, No.101 Longmian Avenue, Nanjing, Jiangsu, P. R. China
[3]Department of Radiology, Affiliated Hospital of Nanjing University of Chinese Medicine, No. 155 Hanzhong Road, Nanjing, Jiangsu, P. R. China

Introduction

Acute pancreatitis (AP) is an inflammatory condition induced by pancreatic enzyme activation, leading to autodigestion of pancreatic tissue. It is one of the most prevalent acute abdominal disorders, with a global incidence of approximately 34 cases per 100,000 people annually, a figure that continues to rise [1, 2]. While the majority of cases (80–85%) are mild and self-limiting, around 20% of patients progress to moderate or severe forms, often accompanied by local and systemic complications. In some cases, multiple organ failure ensues, contributing to high mortality rates [3, 4]. Therefore, the timely and accurate prediction of AP severity is critical for guiding clinical decisions and improving patient outcomes.

Several scoring systems have been developed to assess AP severity, including the Ranson score [5], Acute Physiology and Chronic Health Evaluation (APACHE) II score [6], and Bedside Index for Severity in Acute Pancreatitis (BISAP) score [7], all of which are commonly used in clinical practice. However, both the Ranson and APACHE II scores require multiple parameters and lengthy procedures; for instance, the Ranson score takes up to 48 h post-admission to complete, potentially delaying treatment and reducing its efficacy in early AP severity evaluation. In contrast, the BISAP score offers a simpler and more convenient approach, though its assessment of mental status, one of its components, remains subjective. While the Glasgow Coma Scale could be used for evaluation, it is complex to calculate and less accurate [8]. Recently, efforts have been made to develop new scoring systems based on readily available clinical and laboratory indicators upon patient admission to predict AP severity [9–11]. Nonetheless, these systems often neglect valuable information from imaging, particularly changes within the pancreas itself. Computed tomography (CT), known for its ability to clearly visualize both pancreatic and peripancreatic conditions, is widely employed in diagnosing pancreatitis [12]. Current CT-based scoring systems for AP severity, such as the modified computed tomography severity index (MCTSI), which evaluates pancreatic inflammatory response, pancreatic necrosis, and extrapancreatic complications [13], have demonstrated superior performance compared to the traditional APACHE-II score [14]. However, early imaging often fails to detect pancreatic necrosis, which limits the sensitivity of these scoring systems in the acute phase [15].

Radiomics overcomes the limitations of traditional imaging, which is confined to morphological assessment, by extracting underlying pathophysiological information through quantitative image analysis [16]. Although predominantly employed in cancer-related research [17–19], radiomics has also shown promise in non-tumor studies. Recent advancements have led to the development of radiomics models using enhanced CT or MRI to evaluate the severity of AP [20, 21]. However, routine early enhanced CT is unnecessary for patients with AP [22–24], and MRI is not widely available in primary healthcare settings nor routinely used for AP evaluation.

In response, this study aims to develop an early prediction model for AP severity by integrating clinical parameters with CT radiomics. This model will assist clinicians in identifying patients at risk of progressing to moderately severe acute pancreatitis (MSAP) or severe acute pancreatitis (SAP), thereby enabling timely interventions that could improve patient outcomes.

Methods

Patient selection

A total of 1,035 patients diagnosed with AP at Zhenjiang First People's Hospital between January 2021 and December 2023 were retrospectively reviewed. The diagnosis of AP adhered to the revised 2012 Atlanta classification criteria [25]. The inclusion criteria for the study were: (1) first occurrence of AP, (2) age>18 years, (3) abdominal CT scan within 72 h of symptom onset, and (4) completion of other relevant laboratory tests within 24 h of admission. Exclusion criteria were: (1) time from abdominal pain onset to presentation exceeding 72 h, (2) imaging evidence of chronic pancreatitis (e.g., pancreatic parenchymal atrophy or calcification, irregular dilation of the main pancreatic duct) or a history of pancreatitis, (3) presence of pancreatic tumors or prior pancreatic surgery, (4) incomplete biochemical tests obtained within 24 h or poor-quality CT images, and (5) patients transferred from other hospitals after receiving prior treatment for pancreatitis.

Following the application of these criteria, 245 patients were selected for analysis. These patients were randomly divided into training and validation cohorts at a 7:3 ratio using stratified sampling. A recruitment flowchart is shown in Fig. 1. The study was approved by the hospital's ethics review committee, with a waiver of informed consent.

CT Image acquisition and clinical parameter collection

For CT imaging, patients were positioned supine with their hands raised above their heads for axial abdominal scans using a uCT710 scanner (Shanghai United Imaging Healthcare). The imaging parameters were set as follows: tube voltage of 120 kVp, automatic tube current modulation, slice thickness of 5 mm with 5 mm inter-slice spacing, a field of view of 500 mm × 500 mm, rotation speed of 0.5 s/rotation, pitch of 0.9875, and matrix size of 512×512. Plain CT images were retrospectively retrieved from the Picture Archiving and Communication System (PACS).

Clinical data, including gender, age, etiology, and serological markers (e.g., serum calcium, serum potassium,

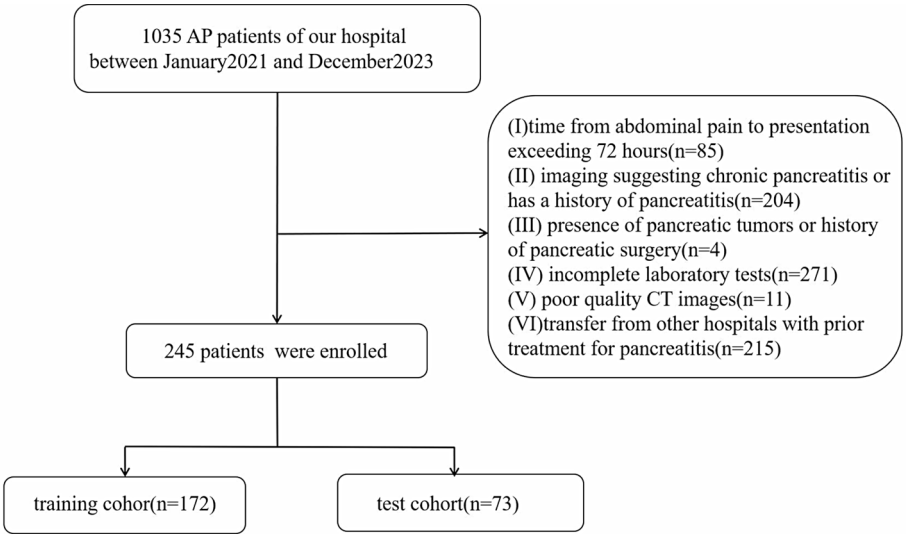

Fig. 1 Workflow of the study: from data collection to model construction and validation

C-reactive protein (CRP), and white blood cell count (WBC)), were collected within the first 24 h of patient admission from the hospital's medical records system. To ensure data accuracy and reliability, two gastroenterologists with over five years of clinical experience conducted the data collection.

Diagnosis criteria and severity assessment of AP

The severity of AP was assessed based on the revised 2012 Atlanta classification [25], which requires at least two of the following three criteria: (1) characteristic abdominal pain indicative of AP; (2) serum amylase or lipase levels exceeding three times the upper normal limit; (3) imaging findings suggestive of AP. Severity was classified as follows: (1) Mild Acute Pancreatitis (MAP): diagnostic criteria for AP are met without organ failure or any local or systemic complications; (2) MSAP: diagnostic criteria for AP are met with temporary organ dysfunction (lasting less than 48 h) or the presence of local or systemic complications; (3) SAP: diagnostic criteria for AP are met with prolonged organ dysfunction (lasting more than 48 h). Organ dysfunction was assessed using the modified Marshall scoring system [25].

Image segmentation and features extraction

Plain CT images were segmented by a radiologist with eight years of experience using ITK-SNAP (version 3.8.0). Regions of interest (ROIs) were manually delineated layer by layer, with a window width of 300 Hu and a window level of 50 Hu, ensuring full coverage of the pancreatic slices while minimizing interference from surrounding blood vessels, bile ducts, and adjacent abdominal structures. The segmented images were resampled to a uniform voxel size of 1 mm × 1 mm × 1 mm. Radiomics features were extracted from each sample using PyRadiomics (https://github.com/Radiomics/pyradiomics) [26], resulting in a total of 1130 features. These included 14 shape features, 18 first-order statistical features, 75 texture features, and 1023 higher-order features. The higher-order features encompassed 18 first-order statistical features with log-sigma transformation, 262 texture features with log-sigma transformation, 18 first-order statistics with wavelet transformation, and 726 texture features with wavelet transformation. The technical workflow for this study is illustrated in Fig. 2.

Inter-observer intraclass correlation coefficient analysis

To ensure the stability and reproducibility of the radiomics features, inter-observer consistency was evaluated using the intraclass correlation coefficient (ICC). A subset of 25 randomly selected samples was re-segmented, and their radiomics features were re-extracted by another senior radiologist. Features exhibiting good consistency (ICC > 0.75) were retained for further analysis.

Feature preprocessing and selection

To minimize the influence of features with varying dimensions, Z-score normalization was applied to the radiomics features in both the training and validation cohorts. Two feature selection methods were employed. Initially, the Mann-Whitney U test was used to compare the severe and non-severe groups in the training set, with features showing no significant differences ($p \geq 0.05$) between the groups excluded. Subsequently, LASSO with 10-fold cross-validation was applied for further dimensionality reduction. By incorporating L1 regularization, LASSO compresses the coefficients of uncorrelated features to zero, effectively performing automatic feature selection. To optimize model performance, the optimal

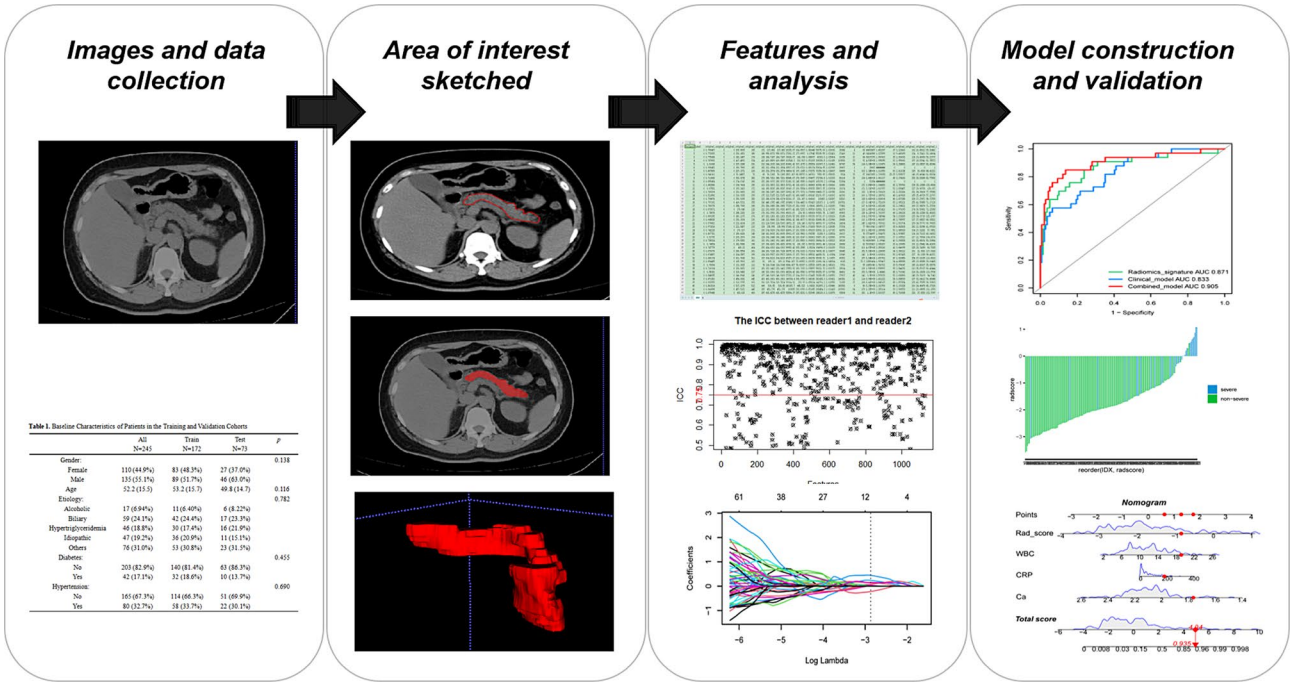

Fig. 2 Case selection flowchart

regularization parameter λ was determined through 10-fold cross-validation. During this process, the coefficients of uncorrelated features progressively shrink as λ increases, and the λ that best optimizes model fit (λ_min) was selected based on the log-likelihood ratio. Features corresponding to non-zero coefficients were retained, resulting in an optimal subset for subsequent modeling and analysis.

Development and validation of models

For the radiomics model, logistic regression was used to develop a radiomics label based on the optimal feature subset from the training set, followed by the calculation of the Rad-score for each sample. Univariate and multivariate logistic regression analyses were performed on the clinical model to identify independent predictors for model construction. In the combined model, independent clinical predictors were integrated with the Rad-score to build the final model, which was visualized using a nomogram. The performance of the radiomics, clinical, and combined models was validated using the validation cohort data.

Statistical analysis

Statistical analyses were conducted using R software (version 3.4.4). Chi-square tests were applied to compare categorical data between groups, while continuous data were analyzed using either the t-test or Mann-Whitney U test, depending on normality and variance homogeneity. To evaluate the performance of the radiomics, clinical, and combined models, the area under the receiver operating characteristic curve (AUC) was calculated. The DeLong test was employed to assess differences between models. Additionally, decision curve analysis (DCA) was conducted to estimate the net benefit at each threshold in both the training and validation cohorts, thereby determining the clinical utility of the models. A p-value of <0.05 was considered statistically significant.

Results

Patient characteristics

Of the 245 participants, 199 were diagnosed with MAP, 20 with MSAP, and 26 with SAP. Patients with MAP were categorized into the non-severe group, consisting of 199 cases, while the severe group comprised 46 cases, including individuals with both MSAP and SAP. Baseline data analysis revealed no significant differences in variables between the training and validation cohorts (Table 1, $p>0.05$). The incidence of severe cases in the overall cohort was 18.8% (46/245), with 18.6% (32/172) in the training cohort and 19.2% (14/73) in the validation cohort.

ICC analysis

Interobserver agreement analysis showed that the median ICC value for all 1130 features was 0.982. Of these, 913 features (80.8%) exhibited an ICC greater than 0.75, indicating strong consistency between operators in delineating the features (Fig. 3).

Table 1 Baseline characteristics of patients in the training and validation cohorts

	All *N* = 245	Train *N* = 172	Test *N* = 73	*p*
Gender				0.138
Female	110 (44.9%)	83 (48.3%)	27 (37.0%)	
Male	135 (55.1%)	89 (51.7%)	46 (63.0%)	
Age	52.2 (15.5)	53.2 (15.7)	49.8 (14.7)	0.116
Etiology				0.782
Alcoholic	17 (6.94%)	11 (6.40%)	6 (8.22%)	
Biliary	59 (24.1%)	42 (24.4%)	17 (23.3%)	
Hypertriglyceridemia	46 (18.8%)	30 (17.4%)	16 (21.9%)	
Idiopathic	47 (19.2%)	36 (20.9%)	11 (15.1%)	
Others	76 (31.0%)	53 (30.8%)	23 (31.5%)	
Diabetes				0.455
No	203 (82.9%)	140 (81.4%)	63 (86.3%)	
Yes	42 (17.1%)	32 (18.6%)	10 (13.7%)	
Hypertension				0.690
No	165 (67.3%)	114 (66.3%)	51 (69.9%)	
Yes	80 (32.7%)	58 (33.7%)	22 (30.1%)	

Feature engineering and model construction

In the univariate analysis, the Mann-Whitney U test identified 435 out of the 913 radiomics features as significantly different between the severe and non-severe groups. Dimensionality reduction was then performed using LASSO regression, which selected 8 features with non-zero coefficients as the optimal subset for model development (Fig. 4). These features included 2 first-order features, 1 texture feature, and 5 wavelet-transformed texture features. A radiomics model was subsequently constructed using logistic regression, and the Rad-score for each sample was calculated (Table 2). The Rad-score was further visualized in a waterfall plot (Fig. 5).

Development of clinical and combined models

For the selection of clinical variables, univariate and multivariate logistic regression analyses identified serum calcium, WBC, and CRP as independent predictors for the severe group (Table 3). Clinical and combined logistic regression models were then constructed based on these independent clinical predictors and the Rad-score, respectively, and visualized through nomograms (Fig. 6).

Model evaluation and clinical application

In the training cohort, the AUC, accuracy, specificity, and sensitivity for the radiomics model, clinical model, and combined model were as follows: 0.871, 0.779, 0.848, and 0.763 (radiomics model); 0.833, 0.651, 0.818, and 0.633 (clinical model); and 0.905, 0.860, 0.848, and 0.863 (combined model). In the validation cohort, the corresponding values were 0.856, 0.700, 0.769, and 0.633 (radiomics model); 0.810, 0.699, 0.846, and 0.667 (clinical model); and 0.908, 0.795, 0.846, and 0.783 (combined model) (Table 4). The ROC curves for the three models in both cohorts are shown in Fig. 7. The DeLong test indicated that the combined model outperformed both the radiomics and clinical models in the training cohort, and in the validation cohort, it surpassed the clinical model (Table 5). DCA analysis demonstrated that the combined model yielded superior clinical net benefits compared to both the radiomics and clinical models across both the training and validation cohorts.

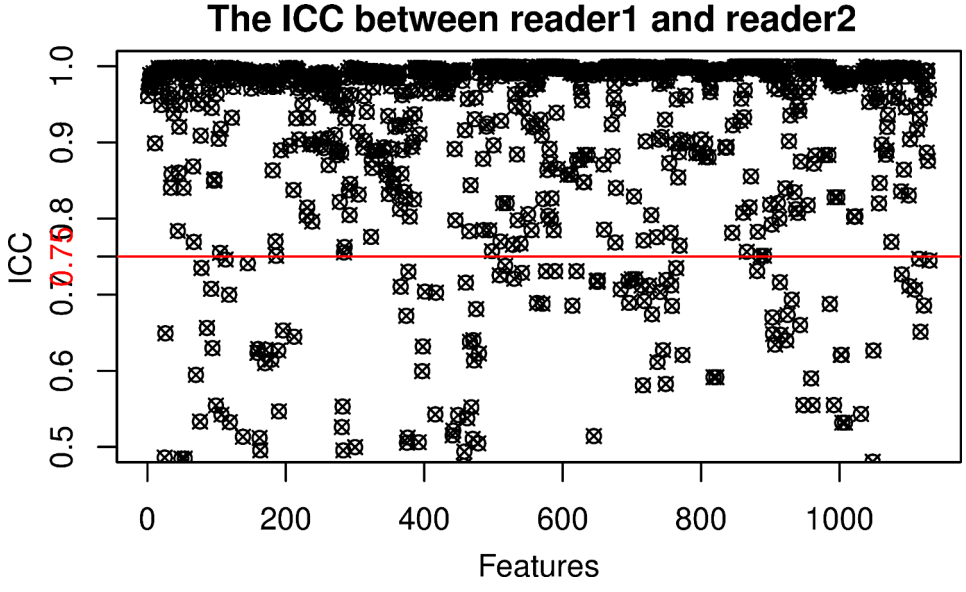

Fig. 3 Inter-observer consistency test of radiomics features. This figure illustrates the inter-observer consistency analysis for radiomics features. The intra-class correlation coefficient (ICC) is computed to evaluate the reproducibility of feature extraction between different observers. Features exhibiting an ICC above 0.75 are retained for subsequent analysis, indicating robust agreement between observers

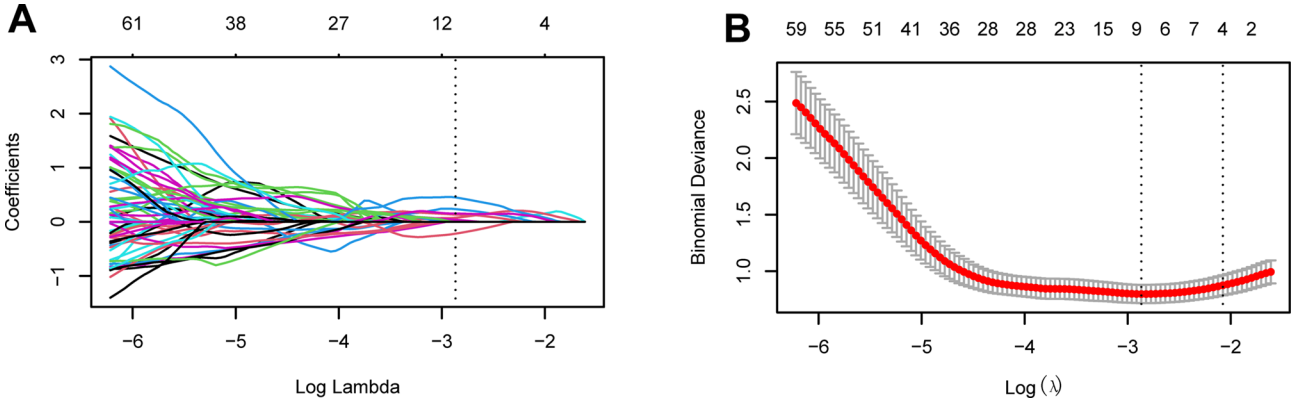

Fig. 4 Least absolute shrinkage and selection operator (LASSO) Regression for Feature Selection. This figure demonstrates the feature selection process. (**A**) The plot depicts the selection of the tuning parameter (λ) through cross-validation. The horizontal axis represents log(λ), while the vertical axis represents binomial deviance. As λ increases, the coefficients of irrelevant features diminish to zero. The optimal λ value, marked by the vertical dashed line, is chosen to balance model complexity and prediction accuracy. (**B**) The coefficient profile plot visualizes the evolution of feature coefficients as the regularization parameter λ is adjusted. Features with non-zero coefficients are retained for the final model

Table 2 Coefficients and corresponding Radiomics features used in the predictive model

Coefficient	Modeling feature
0.234717171	log_sigma_1_mm_3D_firstorder_Mean
0.075021852	log_sigma_1_mm_3D_glszm_LargeAreaEmphasis
0.001774419	log_sigma_3_mm_3D_firstorder_90Percentile
0.039365369	wavelet_HLL_glszm_LargeAreaLowGrayLevelEmphasis
0.132631097	wavelet_HLL_ngtdm_Busyness
-0.220009583	wavelet_LLL_glcm_Imc1
0.450073688	wavelet_LLL_gldm_DependenceNonUniformity
0.153852271	wavelet_LLL_glszm_ZoneEntropy
Constant	-1.706727417

Discussion

This study developed a combined model incorporating CT radiomics features and clinical parameters, providing an individualized approach for early prediction of AP severity. Compared to standalone radiomics and clinical models, the combined model exhibited superior predictive performance, with AUC values of 90.5 and 90.8 in the training and validation cohorts, respectively. In the training cohort, the sensitivity, specificity, and accuracy of the combined model were 0.848, 0.863, and 0.860, respectively, while in the validation cohort, these values were 0.846, 0.783, and 0.795. These results underscore the significant potential of integrating radiomics features with clinical parameters for early prediction of AP severity in clinical practice.

Among the clinical parameters, three independent risk factors—serum calcium, CRP, and WBC—were identified as critical components for the predictive model. Numerous studies have established serum calcium as a reliable

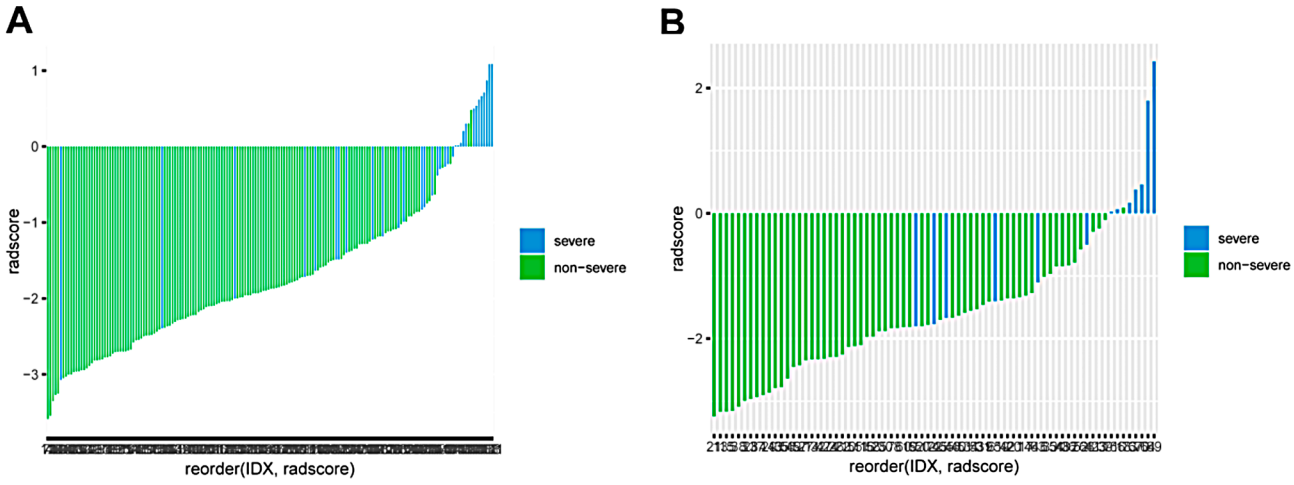

Fig. 5 Waterfall Plot of Radiomics Scores. This figure illustrates the distribution of radiomics scores using a waterfall plot. (**A**) The radiomics scores for the training cohort are presented, showcasing the ranked distribution of scores across the cases. (**B**) The radiomics scores for the validation cohort are displayed, emphasizing the performance consistency between both cohorts. The plot visually highlights the ability of the radiomics signature to distinguish between different outcome groups

Table 3 Results of Univariate and Multivariate analyses for clinical variables

Variables	Univariate analysis			Multivariate analysis		
	B	OR(95% CI)	*p*	B	OR(95% CI)	*p*
Gender	0.139	1.149(0.537–2.462)	0.720			
Age	0.021	1.021(0.996–1.046)	0.096			
Etiology	-0.020	0.980(0.774–1.242)	0.868			
Diabetes	-0.035	0.966(0.362–2.578)	0.945			
Hypertension	0.621	1.860(0.858–4.034)	0.116			
K	0.451	1.569(0.617–3.990)	0.344			
Cl	-0.023	0.977(0.894–1.068)	0.605			
Ca	-6.546	0.001(0.000-0.026)	0.000	-6.558	0.001(0.000-0.141)	0.005
GLU	0.183	1.201(1.087–1.327)	0.000	0.096	1.101(0.953–1.272)	0.191
CRP	0.010	1.010(1.005–1.016)	0.000	0.010	1.011(1.002–1.019)	0.020
WBC	0.186	1.204(1.097–1.322)	0.000	0.149	1.161(1.011–1.333)	0.035
HCT	-0.011	0.989(0.917–1.066)	0.772			
RDW	0.333	1.395(1.009–1.928)	0.044	0.202	1.223(0.842–1.778)	0.291
PLT	0.002	1.002(0.996–1.008)	0.438			
MPV	0.177	1.194(0.914–1.559)	0.194			
PT	0.479	1.615(1.198–2.178)	0.002	-0.072	0.930(0.513–1.688)	0.813
APTT	0.066	1.068(1.007–1.133)	0.027	-0.025	0.975(0.893–1.064)	0.572
TT	0.040	1.041(0.975–1.112)	0.226			
FIB	0.195	1.215(0.982–1.503)	0.073			
DD	0.415	1.515(1.248–1.838)	0.000	0.117	1.124(0.853–1.481)	0.405
TBIL	0.002	1.002(0.985–1.020)	0.805			
DBIL	0.009	1.009(0.987–1.032)	0.437			
IBIL	-0.023	0.978(0.928–1.030)	0.393			
AST	0.002	1.002(1.000-1.004)	0.034	0.000	1.000(0.996–1.004)	0.946
ALT	0.001	1.001(0.999–1.003)	0.236			
ALP	0.003	1.003(0.998–1.008)	0.273			
GGT	0.000	1.000(0.999–1.002)	0.564			
PAB	-0.002	0.998(0.994–1.002)	0.374			
ADA	0.056	1.057(0.984–1.137)	0.130			
LDH	0.004	1.004(1.002–1.006)	0.001	0.003	1.003(1.000-1.006)	0.084
CK	0.001	1.001(0.999–1.003)	0.164			
BUN	0.460	1.584(1.285–1.953)	0.000	0.354	1.424(0.997–2.034)	0.052
CREA	0.018	1.018(1.005–1.032)	0.006	-0.021	0.979(0.956–1.003)	0.088
TP	-0.006	0.994(0.966–1.023)	0.685			
ALB	-0.171	0.843(0.758–0.937)	0.002	-0.030	0.971(0.818–1.152)	0.733
AG	-1.570	0.208(0.062–0.701)	0.011	0.548	1.731(0.319–9.377)	0.525

parameter for predicting AP severity [27–29]. The underlying mechanism is thought to involve autodigestive damage to pancreatic tissue during AP, leading to leakage of pancreatic lipase. This enzyme then interacts with adjacent adipose tissue to release free fatty acids, which enter the bloodstream and bind with calcium ions to form calcium soaps, thus depleting serum calcium and inducing hypocalcemia. The entry of necrotic tissue into the circulation also triggers significant inflammatory responses. Our findings also indicate a positive correlation between CRP and WBC levels with AP severity, consistent with the work of Zerem et al. [30]. It is well established that CRP levels exceeding 150 mg/dL within 48 h of symptom onset are indicative of severe AP [31]. However, due to its nonspecific nature, CRP can be influenced by various other inflammatory conditions. To date, no single laboratory test has proven consistently reliable for accurately predicting the severity of AP [32].

Imaging plays an increasingly pivotal role in the diagnosis and management of AP [33]. Research has demonstrated that microvascular disturbances, progressive tissue ischemia, and reduced perfusion occur early in AP, with microcirculatory dysfunction detectable from the onset [34, 35]. While traditional CT scans primarily reveal morphological changes in the pancreas, radiomics offers the advantage of extracting a comprehensive array of quantitative features from imaging data, revealing details not discernible by the naked eye [36]. In this study, eight significant features were identified, including two first-order features, one texture feature, and

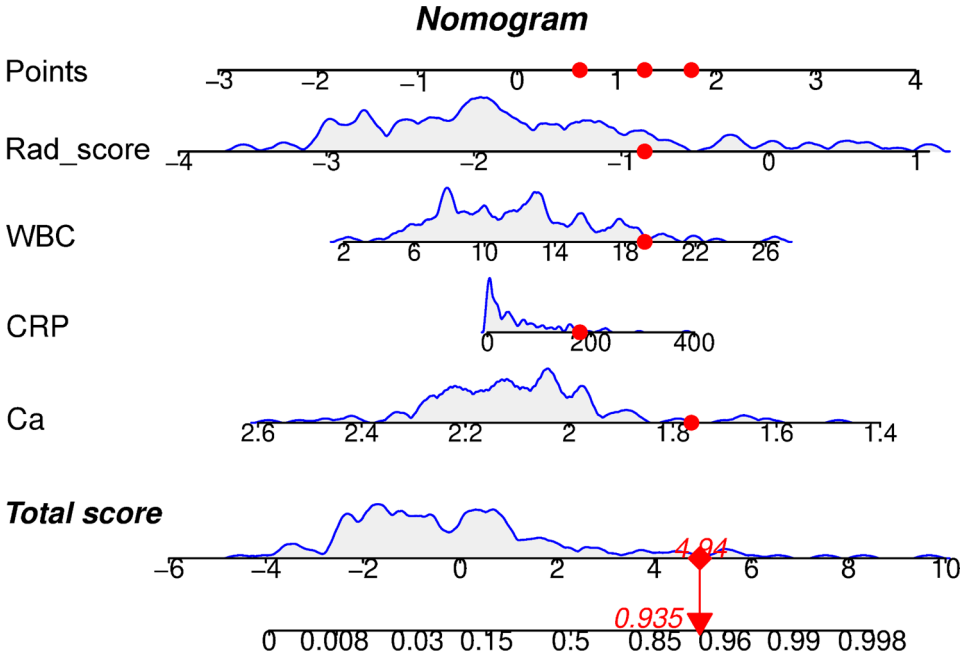

Fig. 6 Nomogram for the clinical-radiomics model. This figure presents the nomogram developed to predict patient outcomes based on the clinical-radiomics model. The nomogram integrates both clinical variables and radiomics features, offering a visual tool to estimate the probability of specific clinical outcomes. Each predictor is assigned a corresponding score, and the cumulative score is used to calculate the likelihood of the outcome, thereby facilitating individualized risk assessment

Table 4 Performance of each model in the training and validation cohorts

Models	Cohorts	AUC (95% CI)	Sensitivity	Specificity	Accuracy
Radiomics model	Training	0.871(0.793–0.949)	0.848	0.763	0.779
	Validation	0.856(0.751–0.967)	0.769	0.633	0.7
Clinical model	Training	0.833(0.756–0.910)	0.818	0.633	0.651
	Validation	0.810(0.692–0.929)	0.846	0.667	0.699
Combined model	Training	0.905(0.837–0.973)	0.848	0.863	0.86
	Validation	0.908(0.824–0.992)	0.846	0.783	0.795

five wavelet-transformed texture features. First-order features, derived from intensity values, encapsulate the overall information of the intensity histogram within the ROI. These features may be indicative of anatomical alterations resulting from microvascular disturbances in pancreatic tissue. Abunahel BM et al. have demonstrated that texture features hold particular significance in the classification and prediction of pancreatic diseases [37]. Wavelet transformations decompose images into multiple frequency bands, which include both low-frequency (L) and high-frequency (H) components. The low-frequency components describe the overall trends and broad changes in the image, while high-frequency components capture more localized features and fine details. Among the features analyzed, the radiomics feature with the largest absolute value was wavelet.LLL_gldm_DependenceNonUniformity. The Gray Level Dependence Matrix (GLDM) is a texture feature that quantifies the gray-level differences between a central voxel and its surrounding voxels, reflecting the distribution of these differences across the image [38]. DependenceNonUniformity specifically measures the non-uniformity of gray-level dependencies within the image, revealing whether the voxel gray-level distribution within the ROI is consistent. This feature suggests that pancreatic tissue changes, such as edema, hemorrhage, and early-stage necrosis, contribute to uneven internal texture, characterized by more chaotic gray levels, increased variation between adjacent gray levels, and a rougher texture. These textural variations are positively correlated with the severity of AP.

CT texture analysis has been widely applied across various diseases, including lung nodules, colorectal cancer, and renal cancer. It has proven effective not only in distinguishing between benign and malignant masses [39–42], thereby enhancing diagnostic accuracy and minimizing unnecessary surgeries, but also in predicting distant metastasis following tumor resection and overall survival [43, 44]. More recently, research has indicated

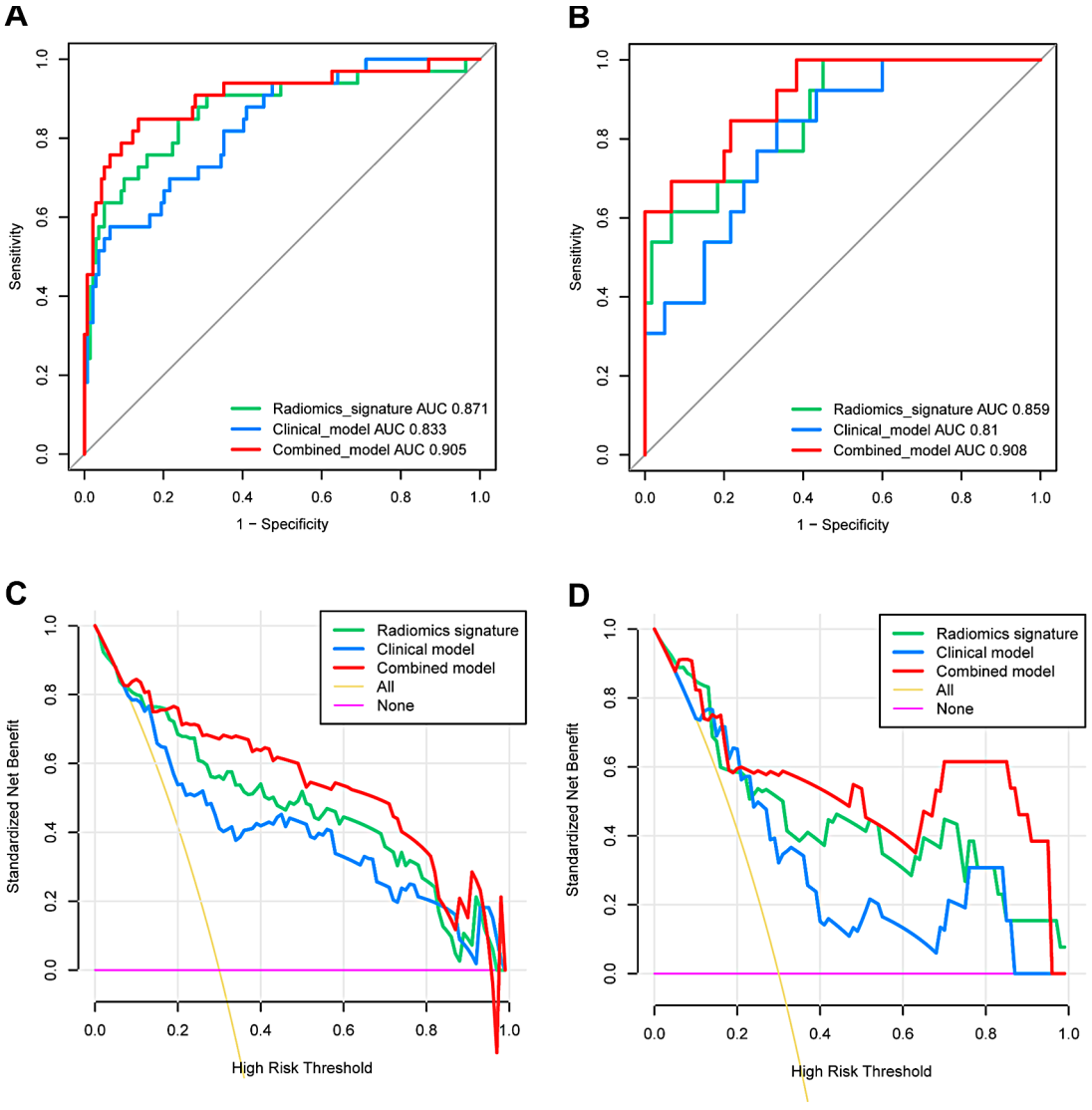

Fig. 7 ROC and Decision Curve Analysis (DCA) curves for the training and validation cohorts. This figure displays multiple ROC and DCA curves, comparing the Radiomics model, Clinical model, and Combined model. (**A, C**) In the training cohort, ROC curves demonstrate the discriminative ability of the Radiomics model, Clinical model, and Combined model, while the corresponding DCA curves illustrate the clinical utility of these models. (**B, D**) In the validation cohort, ROC curves evaluate the performance of the three models, and DCA curves assess their clinical net benefit across varying threshold probabilities.

Table 5 ROC comparison between radiomics signature, clinical model, and combined model in the training and validation cohorts using DeLong test

Cohorts	ROC1	ROC2	*p*
Training	Radiomics_signature	Clinical_model	0.399997177
	Radiomics_signature	Combined_model	0.038678276
	Clinical_model	Combined_model	0.043489261
Validation	Radiomics_signature	Clinical_model	0.498226072
	Radiomics_signature	Combined_model	0.228744892
	Clinical_model	Combined_model	0.018904571

that textural features can assist in predicting molecular subgroups of tumors [45–47].

Several studies have investigated AP using radiomics [48–50]. Hu et al. [48] utilized 3D radiomics features from T2-weighted MRI combined with clinical data to predict AP recurrence. Xue et al. [49] applied CT radiomics for predicting AP prognosis, while Liu et al. [50] developed a clinical-radiomics model to forecast the risk of persistent organ failure in patients with acute necrotizing pancreatitis. Additionally, other studies have focused on predicting AP severity. Zhao et al. [20] proposed a radiomics model based on enhanced CT images from the pancreatic and peripancreatic portal venous phase to predict AP severity, achieving an AUC of 0.965, which surpasses the

performance of the present study. Lin et al. [21] identified 11 potential features from enhanced MR imaging to develop a radiomics model with an AUC of 0.848, slightly lower than that reported here. This study presents two key advantages over previous research. First, radiomics features were extracted from non-enhanced CT images, acknowledging that most patients with AP do not undergo enhanced CT scans during the early stages of the disease. Furthermore, MRI is cost-prohibitive, less practical in emergency settings, and not widely accessible in primary hospitals, rendering this study more clinically applicable. Second, the study integrated radiomics features with independent clinical predictors, incorporating both localized and systemic information to construct an individualized predictive model, thereby enhancing its reliability. Our early combined prediction model performed well for 3 reasons: first, consistent scanning instruments and modalities across all patients ensured imaging parameter uniformity; second, image resampling to a uniform voxel size guaranteed spatial consistency; and third, the model incorporated both local information from altered pancreatic parenchyma and systemic data derived from abnormal blood parameters, combining the two to improve model comprehensiveness and efficacy.

Nevertheless, certain limitations exist in our current study. First, it is a single-center retrospective study, which may affect the generalizability of the model. Future multicenter, large-sample prospective studies are needed to validate the generalizability and stability of the combined model. Second, while the model effectively predicts severe AP (encompassing MSAP and SAP), it does not distinguish between these two subgroups. Patients with SAP often experience persistent multi-organ failure and higher mortality rates compared to patients with MSAP, indicating that future studies should focus on predicting MSAP and SAP separately. Finally, radiomics research currently relies on manual delineation as the gold standard for image annotation, a process that is time-intensive. Future work should explore automated delineation techniques to streamline model development.

In conclusion, an individualized model was developed incorporating CT radiomics features and independent clinical predictors, aiding clinicians in the prompt and accurate assessment of AP severity. This model facilitates personalized and precise treatment, ultimately improving patient outcomes.

Acknowledgements
Not applicable.

Author contributions
QMY contributed to the conception and design of the study, played a significant role in the acquisition, analysis, and interpretation of data, and were involved in drafting the manuscript and revising it critically for important intellectual content. DR and LC was involved in the analysis and interpretation of the data, particularly focusing on the radiomics aspect, and contributed to the manuscript by revising critically for important intellectual content. ZJL participated in the acquisition of data and provided technical or material support. They also contributed to the drafting and critical revision of the manuscript. SXH and HH contributed to the conception and design of the study, supervise the entire project, and were involved in drafting the manuscript and revising itcritically for important intellectual content. Their leadership in project administration and supervision played a crucial role in the study's success. All authors approved the final version of the manuscript and agree to be accountable for all aspects of the work in ensuring that questions related to the accuracy or integrity of any part of the work are appropriately investigated and resolved.

Funding
This study was funded by the 2023 Special Project of Zhenjiang Key Laboratory of Health and Life Science (GZsYS202302) and the Research Fund Project of Jiangsu University Affiliated People's Hospital (Y2021011-S, Y2022024).

Data availability
The materials and data are available from the corresponding author on specific request.

Declarations

Ethical approval
The research involving clinical images was approved by the Ethics Committee of the Affiliated People's Hospital of Jiangsu University. Written informed consent was not required due to the retrospective nature of the study.

Consent for publication
Not Applicable.

Clinical trial number
Not applicable

Competing interests
The authors declare no competing interests.

Received: 1 October 2024 / Accepted: 21 November 2024
Published online: 27 November 2024

References

1. Lankisch PG, Apte M, Banks PA. Acute pancreatitis. Lancet (London England). 2015;386(9988):85–96.
2. Xiao A Y, Tan M L, Wu L M, et al. Global incidence and mortality of pancreatic diseases: a systematic review, meta-analysis, and meta-regression of population-based cohort studies. Volume 1. The lancet Gastroenterology & hepatology; 2016. pp. 45–55. 1.
3. Schepers NJ, Bakker OJ, Besselink MG, et al. Impact of characteristics of organ failure and infected necrosis on mortality in necrotising pancreatitis. Gut. 2019;68(6):1044–51.
4. Garg PK, Singh VP. Organ failure due to systemic Injury in Acute pancreatitis. Gastroenterology. 2019;156(7):2008–23.
5. Ranson JH, Rifkind KM, Roses DF, et al. Objective early identification of severe acute pancreatitis . Am J Gastroenterol. 1974;61(6):443–51.
6. Al-Hadeedi S, Fan ST, Leaper D. APACHE-II score for assessment and monitoring of acute pancreatitis. Lancet (London England). 1989;2(8665):738.
7. Gao W, Yang HX, Ma CE. The value of BISAP score for Predicting Mortality and Severity in Acute Pancreatitis: a systematic review and Meta-analysis. PLoS ONE. 2015;10(6):e0130412.
8. Bledsoe BE, Casey MJ, Feldman J, et al. Glasgow Coma Scale Scoring is often inaccurate. Prehosp Disaster Med. 2015;30(1):46–53.
9. He SS, Li D, He QY et al. Establishment of Early Multi-Indicator Prediction Models of Moderately Severe Acute Pancreatitis and Severe Acute Pancreatitis. Gastroenterology research and practice, 2022, 2022: 5142473.
10. Li B, Wu W. Establishment and validation of a Nomogram Prediction Model for the severe Acute pancreatitis. J Inflamm Res. 2023;16:2831–43.

11. He Q, Ding J. The predictive value of procalcitonin combined with C-reactive protein and D dimer in moderately severe and severe acute pancreatitis. Eur J Gastroenterol Hepatol. 2022;34(7):744–50.
12. Ortiz Morales CM, Girela Baena EL, Olalla Muñoz JR, et al. Radiology of acute pancreatitis today: the Atlanta classification and the current role of imaging in its diagnosis and treatment. Radiologia. 2019;61(6):453–66.
13. Mortele KJ, Wiesner W. A modified CT severity index for evaluating acute pancreatitis: improved correlation with patient outcome. AJR Am J Roentgenol. 2004;183(5):1261–5.
14. Alberti P, Mata Pandoe. Evaluation of the modified computed tomography severity index (MCTSI) and computed tomography severity index (CTSI) in predicting severity and clinical outcomes in acute pancreatitis. J Dig Dis. 2021;22(1):41–8.
15. Shinagare A B, IP I K Rajaas, et al. Use of CT and MRI in emergency department patients with acute pancreatitis. Abdom Imaging. 2015;40(2):272–7.
16. Gillies RJ, Kinahan PE, Hricak H, Radiomics. Images are more than pictures. They Are Data Radiol. 2016;278(2):563–77.
17. Gillies RJ, Schabath MB. Radiomics improves Cancer Screening and early detection. Cancer epidemiology, biomarkers & prevention: a publication of the American Association for Cancer Research. Cosponsored Am Soc Prev Oncol. 2020;29(12):2556–67.
18. Sun Q, Chen Y, Liang C, et al. Biologic pathways underlying prognostic Radiomics phenotypes from paired MRI and RNA sequencing in Glioblastoma. Radiology. 2021;301(3):654–63.
19. Liu F, Zhao Y, Song J, et al. A hybrid classification model with radiomics and CNN for high and low grading of prostate cancer Gleason score on mp-MRI. Displays. 2024;83:102703.
20. Zhao Y, Wei J. Early prediction of acute pancreatitis severity based on changes in pancreatic and peripancreatic computed tomography radiomics nomogram. Quant Imaging Med Surg. 2023;13(3):1927–36.
21. Lin Q, Ji YF, Chen Y, et al. Radiomics model of contrast-enhanced MRI for early prediction of acute pancreatitis severity. J Magn Reson Imaging: JMRI. 2020;51(2):397–406.
22. Tenner S, Baillie J, Dewitt J, et al. American College of Gastroenterology guideline: management of acute pancreatitis. Am J Gastroenterol. 2013;108(9):1400–15.
23. IAP/APA evidence-based guidelines for the management of acute pancreatitis. Pancreatology: Official J Int Association Pancreatology (IAP) [et al]. 2013;13(4 Suppl 2):e1–15.
24. Huang H, Chen W, Tang G, et al. Optimal timing of contrast-enhanced computed tomography in an evaluation of severe acute pancreatitis-associated complications. Experimental Therapeutic Med. 2019;18(2):1029–38.
25. Banks P A, Bollen T L, Dervenis C, et al. Classification of acute pancreatitis–2012: revision of the Atlanta classification and definitions by international consensus. Gut. 2013;62(1):102–11.
26. Van Griethuysen JJM, Fedorov A, Parmar C, et al. Computational Radiomics System to Decode the Radiographic phenotype. Cancer Res. 2017;77(21):e104–7.
27. Ye JF, Zhao YX Ju J, et al. Building and verifying a severity prediction model of acute pancreatitis (AP) based on BISAP, MEWS and routine test indexes. Clin Res Hepatol Gastroenterol. 2017;41(5):585–91.
28. Liu GH, Chen J, Li LQ, et al. Development and validation of a nomogram for early assessment the severity of acute pancreatitis. Scand J Gastroenterol. 2022;57(8):990–5.
29. Cao X, Wang HM, Lu R, et al. Establishment and verification of a nomogram for predicting severe acute pancreatitis. Eur Rev Med Pharmacol Sci. 2021;25(3):1455–61.
30. Zerem D, Zerem O. Role of clinical, biochemical, and Imaging parameters in predicting the severity of Acute pancreatitis . Euroasian J hepato-gastroenterology. 2017;7(1):1–5.
31. Staubli SM, Nebiker C Oertlid. Laboratory markers predicting severity of acute pancreatitis. Crit Rev Clin Lab Sci. 2015;52(6):273–83.
32. Leppäniemi A, Tolonen M. 2019 WSES guidelines for the management of severe acute pancreatitis. World J Emerg Surgery: WJES. 2019;14:27.
33. Thoeni RF. The revised Atlanta classification of acute pancreatitis: its importance for the radiologist and its effect on treatment. Radiology. 2012;262(3):751–64.
34. Smeets X, Litjens G, Gijsbers K, et al. The accuracy of pancreatic perfusion computed Tomography and Angiography in Predicting Necrotizing pancreatitis: a systematic review. Pancreas. 2018;47(6):667–74.
35. Singh VK, Wu BU, Bollentl, et al. Early systemic inflammatory response syndrome is associated with severe acute pancreatitis. Clin Gastroenterol Hepatology: Official Clin Pract J Am Gastroenterological Association. 2009;7(11):1247–51.
36. Lambin, P, Leijenaar RTH, Deist TM, et al. Radiomics: the bridge between medical imaging and personalized medicine. Nat Reviews Clin Oncol. 2017;14(12):749–62.
37. Abunahel BM, Pontre B, Kumar H, et al. Pancreas image mining: a systematic review of radiomics. Eur Radiol. 2021;31(5):3447–67.
38. He W, Tang M, Jiang X, et al. Visual interpretation of Radiomics Features in filtered computed tomography images during the Portal Phase of Acute pancreatitis. Discov Med. 2024;36(183):730–8.
39. Liu C, Ma C, Duan J, et al. Using CT texture analysis to differentiate between peripheral lung cancer and pulmonary inflammatory pseudotumor [J]. BMC Med Imaging. 2020;20(1):75.
40. Wang Q, Xu S, Zhang G, et al. Applying a CT texture analysis model trained with deep-learning reconstruction images to iterative reconstruction images in pulmonary nodule diagnosis. J Appl Clin Med Phys. 2022;23(11):e13759.
41. Valletta R, Faccioli N, Bonatti M, et al. Role of CT colonography in differentiating sigmoid cancer from chronic diverticular disease. Japanese J Radiol. 2022;40(1):48–55.
42. Wang X, Yuan M, Mi H, et al. The feasibility of differentiating colorectal cancer from normal and inflammatory thickening colon wall using CT texture analysis. Sci Rep. 2020;10(1):6346.
43. Zhao Y, Liu G, Sun Q, et al. Validation of CT radiomics for prediction of distant metastasis after surgical resection in patients with clear cell renal cell carcinoma: exploring the underlying signaling pathways. Eur Radiol. 2021;31(7):5032–40.
44. Lu N, Zhang WJ, Dong L, et al. Dual-region radiomics signature: integrating primary tumor and lymph node computed tomography features improves survival prediction in esophageal squamous cell cancer. Volume 208. Computer methods and programs in biomedicine; 2021. p. 106287.
45. Li ZC, Bai H, Sun Q, et al. Multiregional radiomics profiling from multiparametric MRI: identifying an imaging predictor of IDH1 mutation status in glioblastoma. Cancer Med. 2018;7(12):5999–6009.
46. Yan J, Liu L, Wang W, et al. Radiomic features from Multi-parameter MRI Combined with Clinical parameters Predict Molecular subgroups in patients with medulloblastoma. Front Oncol. 2020;10:558162.
47. Liu Z, Hong X. Radiomic features from multiparametric magnetic resonance imaging predict molecular subgroups of pediatric low-grade gliomas. BMC Cancer. 2023;23(1):848.
48. Hu Y, Liu N. Three-Dimensional Radiomics features of magnetic resonance T2-Weighted imaging combined with clinical characteristics to predict the recurrence of Acute pancreatitis. Front Med. 2022;9:777368.
49. Xue M, Lin S, Xie D, et al. The value of CT-based radiomics in predicting the prognosis of acute pancreatitis. Front Med. 2023;10:1289295.
50. Liu N, Wan Y, Tong Y et al. A Clinic-radiomics model for predicting the incidence of persistent organ failure in patients with acute necrotizing pancreatitis. Gastroenterology research and practice, 2023, 2023: 2831024.

Publisher's note